Eur. Phys. J. A (2019) **55**: 69
DOI 10.1140/epja/i2019-12741-3

THE EUROPEAN PHYSICAL JOURNAL A

Regular Article – Theoretical Physics

Transverse momentum distribution of charged hadrons based on wounded quark model

P.K. Srivastava[1,a], Arpit Singh[2,b], O.S.K. Chaturvedi[2], P.K. Raina[1,c], and B.K. Singh[2,d]

[1] Department of Physics, Indian Institute of Technology Ropar, Rupnagar-140001, India
[2] Department of Physics, Institute of Science, Banaras Hindu University, Varanasi-221005, India

Received: 22 December 2018 / Revised: 19 March 2019
Published online: 15 May 2019

Communicated by G. Torrieri

Abstract. In nucleus-nucleus collisions, new particles are produced mainly through strong interactions among the constituents of the QCD medium. The search of a unified phenomenological model to understand this production mechanism is one of the main motivation behind the heavy ion experiments. A vast variety of data coming from nucleus-nucleus collision experiments put a stringent constraint on the particle production models. A unified and proper model must satisfy the various data regarding pseudorapidity distributions, transverse energy density distributions, transverse momentum distributions with respect to control parameters in different types of collisions at various energies simultaneously. Recently we proposed a new version of wounded quark model (WQM) which actually satisfies many points of this criteria. However, these kind of static initial model conditions have problem in calculating the transverse momentum distributions of charged hadrons. In this article, we have used the important ingredients of WQM like number of wounded quarks and number of quark-quark collisions to fit the transverse momentum spectra of charged hadrons. Based on the assumption of different mechanisms at different regions, *i.e.* different mechanisms for soft p_T and hard momentum part, we have proposed a parameterization made of two functions to calculate the transverse momentum spectra in different collisions at different energies ranging from higher RHIC to LHC. We hope that this study along with our recent work on WQM will become a more suitable choice as unified model for particle production in strong interaction, instead of wounded nucleon model.

1 Introduction

The study of particle production in nucleus-nucleus collisions is crucial to understand the properties and behaviour of quantum chromodynamics (QCD) [1–3]. Further this study is able to confirm the existence of various theoretically stated phases of the QCD matter. We know that the particle production process in these collisions is non-perturbative at low momenta and therefore it is theoretically difficult to obtain this soft hadron production directly from perturbative QCD. On the other side perturbative methods have shown their ability at large momenta to calculate the hadron production in nucleus-nucleus collisions. There are limitations on lattice methods to calculate the particle production in soft regime due to its non-perturbative feature. Thus, a lot of efforts have been made to construct a phenomenological model to calculate various distributions of charged hadrons and which efficiently matched with the experimental data.

Transverse momentum of charged hadrons is an important tool to understand the magnitude of temperature of the collision zone from where they have been created [4, 5]. Further transverse momentum spectra (p_T-spectra) are useful to understand the evolution dynamics of the medium [6,7]. This observable help us to find the collective flow of the medium formed during the heavy-ion collisions. In hadronic collisions, the invariant cross-section for charged hadron production with respect to p_T and center-of-mass energy ($\sqrt{s_{NN}}$) has a characteristic shape. At low p_T, the shape is exponential and almost independent of $\sqrt{s_{NN}}$. This region is known as soft physics region where hadrons are fragments of "beam jets" [8,9]. At higher p_T side, this distribution has a power-law tail which strongly depends on $\sqrt{s_{NN}}$. This is hard-scattering region where the charged hadrons are basically produced from high momentum QCD jets. Further the inclusive p_T-spectrum

[a] e-mail: prashant.srivastava@iitrpr.ac.in
[b] e-mail: arpit.singh@bhu.ac.in
[c] e-mail: pkraina@iitrpr.ac.in
[d] e-mail: bksingh@bhu.ac.in

in nucleus-nucleus collisions can be affected by many aspects of collision dynamics. The p_T-distribution function in nucleus-nucleus collisions includes soft parton scattering followed by longitudinal or "string" fragmentation and hard parton scattering followed by transverse fragmentation. Therefore the structure of p_T spectrum in nucleus-nucleus collisions which strongly depends on the particle production mechanism, becomes complex interplay of various physical mechanisms.

A lot of effort has been put forward to unfold and interpret the structure of p_T distribution function of charged hadrons in nucleus-nucleus collisions. Earlier it was supposed that due to thermalization of the QCD medium, the p_T-spectra of the produced particles will follow an exponential distribution with respect to p_T [10,11]. Later, the data from nucleus-nucleus collision experiments shows that exponential function is unable to accommodate the charged hadrons with high p_T. Based on some recent works, practitioners in this field have suggested that the particle production mechanism in different p_T region is different and thus p_T-distribution changes its nature from exponential at low p_T to power-law at large p_T [12]. In other works, it has been shown that the p_T-spectra of charged hadrons satisfy the Tsallis distribution function [13–18]. Tsallis function assumes that this behaviour of p_T-spectra is due to the intrinsic, non-statistical fluctuations [19,20]. Tsallis function fits the p_T-spectra of charged hadron quite well but with some shortcomings. To fit the invariant yield using Tsallis function, we need 3 parameters for 200 GeV data, 4 parameters for 2.76 TeV data [21] and Tsallis function is not able to fit the 5.02 TeV data [22]. Thus we cannot use Tsallis function with definite set of parameters to fit the invariant yield data at each collision energies simultaneously. Further the physical significance of these parameters are not quite well understood. There are other efforts as well however one can see that there exist a lot of open questions in this field. For example, we know that hard parton scattering is expected to dominate the spectrum at larger p_T at high energies but how does hard scattering contribute at smaller p_T and how does it interact with thermal or "soft" particle production [23–25]. The answers of these questions are still not known. Keeping these questions in mind and based on inputs from some recent studies, we have constructed an expression by blending exponential function at low p_T and power law at high p_T to calculate the p_T-spectra of charged hadrons. The new and interesting feature of our work is that we have used the number of wounded quarks (N_q^{AB}) and mean number of quark collisions (ν_q^{AB}) from our wounded quark model (WQM) [26–33] in these functions. Some of the recent experimental and theoretical works favour wounded quark picture over wounded nucleon picture. The authors in ref. [34] have shown that the charged particle multiplicity density at mid-rapidity in Au+Au collisions scales linearly with the number of participating constituent quarks. Further, same behaviour has been observed by wounded quark model for Au+Au collisions at 200 GeV and Pb+Pb collisions at 2.76 TeV [28]. WQM also predicts scaling with constituent quarks for U+U collisions at 193 GeV [32]. The PHENIX Collaboration results [35] support the model results and confirms that mid-rapidity multiplicity data is better described by scaling with the number of constituent quark participants than scaling with the number of participants. Further, the PHENIX Collaboration results [35, 36] show that the transverse energy distribution at mid-rapidity also scales with the number of constituent quark participants. The authors in ref. [32] have shown the scaling behaviour of transverse energy density with participating quarks for U + U collisions at 193 GeV. Apart from scaling of mid-rapidity data with the number of participating quarks, STAR Collaboration [37] have reported that elliptic flow as a function of transverse momentum scales with the number of constituent quarks. Further, the scaling of elliptic flow with number of constituent quarks has been also observed for different collision systems and particle species [38–40]. Recently, Bożek and Broniowski [41] reported the results on transverse momentum fluctuations in p + Pb and Pb + Pb collisions by combining wounded quarks with viscous hydrodynamics. They found a significantly better agreement with the experimental data in the model with wounded quarks than with nucleon participants. The result further favours the use of sub-nucleonic degrees of freedom in the early dynamics of the system formed in ultrarelativistic nuclear collisions. Thus, in this paper we have used WQM where quark-quark interaction is used as the basic ingredient for particle production mechanism. We used this wounded quark picture to fit the invariant yield of charged hadrons produced in various heavy ion collisions.

The rest of the paper is organized as follows: in sect. 2, we start with a brief discussion about the calculation of number of participating quarks, mean number of quark collisions and pseudorapidity density of charged hadrons in WQM. Then we discuss about the parametrization for transverse momentum distribution of charged hadrons using inputs from WQM. In sect. 3 we will discuss the results consisting transverse momentum spectra of charged hadrons in different collisions at various collision energies. At last we will summarize our present work.

2 Model formalism

2.1 Wounded quark model

Recently, we have proposed a new version of wounded quark model based on the phenomena of gluon exchange between the projectile and target quarks with a simple assumption that all the quark collisions are independent and their effects are coherently superimposed. We have used two component model of pseudorapidity distribution in nucleus-nucleus collisions in the wounded quark scenario. We assume that the hard component scales with the number of quark-quark collisions ($N_q^{AB}\nu_q^{AB}$) and the soft component scales with the number of participating quarks (N_q^{AB}). Thus, the expression for pseudorapidity density at midrapidity in $A-B$ collisions can be parameterized in

terms of $p-p$ rapidity density [26,27] as:

$$\left(\frac{\mathrm{d}n_{ch}}{\mathrm{d}\eta}\right)_{\eta=0}^{AB} = \left(\frac{\mathrm{d}n_{ch}}{\mathrm{d}\eta}\right)_{\eta=0}^{pp} \left[(1-x)\, N_q^{AB} + x N_q^{AB} \nu_q^{AB}\right]. \tag{1}$$

Here, x quantifies the relative contributions of hard and soft components. Within the framework of Additive Quark Model [42–46], the mean number of inelastic quark collision (ν_q^{AB}) and the mean number of participating quarks (N_q^{AB}) can be expressed, respectively, as

$$\nu_q^{AB} = \nu_{qA}\nu_{qB} = \frac{A\sigma_{qN}^{in}}{\sigma_{qA}^{in}} \cdot \frac{B\sigma_{qN}^{in}}{\sigma_{qB}^{in}}, \tag{2}$$

$$N_q^{AB} = \frac{1}{2}\left[\frac{N_B\sigma_{qA}^{in}}{\sigma_{AB}^{in}} + \frac{N_A\sigma_{qB}^{in}}{\sigma_{AB}^{in}}\right]. \tag{3}$$

Here, quark-nucleus inelastic cross-section (σ_{qA}^{in}) is determined by using Glauber's approximation [47,48] and nucleus-nucleus inelastic cross-section (σ_{AB}^{in}) can be expressed as

$$\sigma_{AB}^{in} = \pi r^2 \left[A^{1/3} + B^{1/3} - \frac{c}{A^{1/3}+B^{1/3}}\right]^2, \tag{4}$$

where the constant c has a fixed value for nucleus-nucleus collisions and is related with the mean free path of a nucleon inside a nucleus.

2.2 Parameterization of transverse momentum distribution

Our parameterization of transverse momentum spectrum for charged hadrons is based on the idea of modified multi-pomeron exchange model [49–55]. In the modified multi-pomeron exchange model with string fusion for $p-p$ collisions, the expression of transverse spectrum for charged hadrons from one string is as follows [56]:

$$\frac{\mathrm{d}^2N_{ch}}{\mathrm{d}p_T^2} \sim \exp\frac{-\pi(p_T^2+m^2)}{t}, \tag{5}$$

where t measures the color string tension. According to this multi-pomeron exchange model, increase in collision energy causes a general growth in the number of multi-pomerons exchange in nucleon-nucleon collisions.

We have assumed a similar kind of situation where a color string has been formed due to exchange of gluons between quarks in $p-p$ collisions and as the collision energy increases the number of exchanged gluons also increases. Consequently, the number of strings will increase and they start to overlap causing a higher string tension according to string fusion model. However, we are different from multi-pomeron exchange model as we have taken two different functions in two p_T regions. In this study, we have parameterized the p_T-spectra of produced charged hadrons by blending exponential and power law functions in low p_T region ($p_T \le p_{th}$) and high p_T region ($p_T > p_{th}$), respectively. Based on these assumptions, our new parameterization for the p_T-spectrum of charged hadrons in low p_T region for $p-p$ collisions are as follows:

$$E\frac{\mathrm{d}^3N}{\mathrm{d}p^3} = \frac{P_1}{2\pi p_T^2}\left[\exp\left(-\frac{m_T^2}{P_2\sqrt{s_a}}\right) + \frac{P_3}{m_T}\right], \quad p_T \le p_{th} \tag{6}$$

and in high p_T region, the relation can be given by a power law function as follows:

$$E\frac{\mathrm{d}^3N}{\mathrm{d}p^3} = \frac{1}{2\pi p_T^2}\left(\frac{m_T^2}{P_4\sqrt{s_a}}\right)^{-P_5}, \quad p_T > p_{th}. \tag{7}$$

Further, we have extended our model to fit the transverse momentum spectrum of charged hadrons in nucleus-nucleus collisions based on the assumptions of WQM [27]. In the low p_T region, the relation for invariant yield for charged hadrons can be expressed as

$$E\frac{\mathrm{d}^3N}{\mathrm{d}p^3} = \frac{P_1}{2\pi p_T^2}\left[\exp\left(-\frac{m_T^2 N_q^{AB}}{P_2(\nu_q^{AB}s_a)^{1/2}}\right) + \frac{P_3}{m_T}\right], \quad p_T \le p_{th} \tag{8}$$

and by a power law function in high p_T region as

$$E\frac{\mathrm{d}^3N}{\mathrm{d}p^3} = \frac{1}{2\pi p_T^2}\left(\frac{m_T^2 N_q^{AB}}{P_4(\nu_q^{AB}s_a)^{1/2}}\right)^{-P_5}, \quad p_T > p_{th}, \tag{9}$$

where P_1, P_2, P_3, P_4, and P_5 are the fitting parameters, m_T ($=\sqrt{p_T^2+m^2}$) is the transverse mass of the particles produced in nucleus-nucleus collisions, $\sqrt{s_a}$ is the available center of mass energy in nucleus-nucleus collisions.

3 Results and discussions

3.1 Transverse momentum distributions

In this section we have shown the experimental data for invariant yield of charged hadrons in proton-proton and nucleus-nucleus collisions with respect to p_T and fitted these experimental data using respective parameterizations. Before presenting the model results, we want to show the intermediate p_T point where soft and hard part meets. For this exercise, we have plotted fig. 1. In fig. 1, we have shown the invariant yield of charged hadrons produced in most central Pb + Pb collisons at $\sqrt{s_{NN}} = 2.76\,\mathrm{TeV}$ and 5.02 TeV. We have fitted the low p_T region with exponential function as given by eq. (8) and high p_T data with power law as given by eq. (9). We define p_{th} as the intersection point of exponential and power law fitting functions. In fig. 2, we have demonstrated the variation of normalized transverse momentum spectrum of charged hadrons in $p+p$ collisions at $\sqrt{s_{NN}} = 200\,\mathrm{GeV}$, 2.76 TeV and 5.02 TeV with respect to p_T. We have fitted the experimental data [57–59] using our parameterization in eqs. (6) and (7). One can see that as the energy increases, the range of p_T distribution increases from 10 GeV

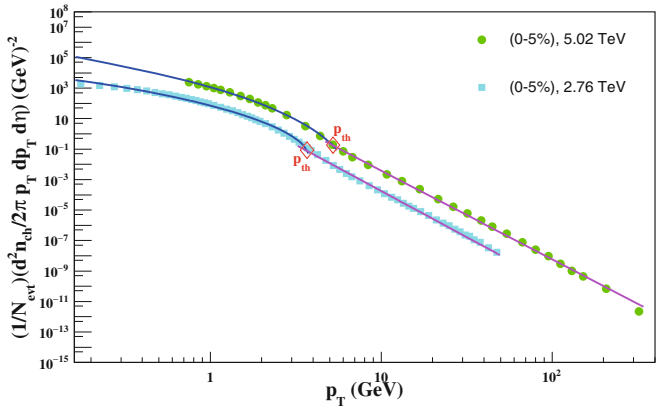

Fig. 1. (Color online) Experimental data of invariant yield of charged hadrons for Pb + Pb collisions at 2.76 and 5.02 TeV with respect to p_T. Violet line shows the exponential fit and pink line shows the power law fit.

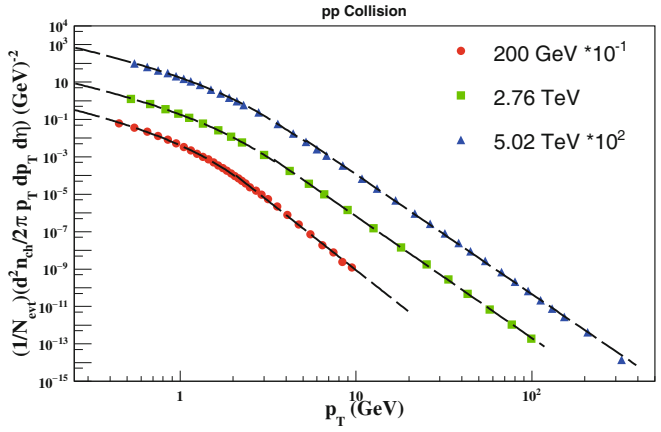

Fig. 2. (Color online) Variation of invariant yield of charged hadrons produced in $p+p$ collisions at three different energies *i.e.*, 200 GeV, 2.76 TeV and 5.02 TeV with respect to transverse momentum (p_T). The experimental data used here are taken from refs. [57–59].

to 300 GeV, which means that the charged hadrons having higher and higher p_T are started to produce. Our parameterization fits the data at each energies simultaneously. The parameters are shown in table 1.

In fig. 3, we have plotted the variation of normalized transverse momentum spectrum of charged hadrons in Cu + Cu collisions at $\sqrt{s_{NN}} = 200$ GeV with p_T. We have fitted the experimental data [60] with exponential function at lower p_T and power law at larger p_T as given by eqs. (8) and (9), respectively. We have fixed the higher limit of p_T for exponential or lowest limit of p_T for power law by simply observing the value of p_T at which these two functions joined smoothly. This region of transverse momentum can be called as intermediate p_T where both hard and soft part contribute. We have done the fitting for different centrality class and found that our parameterization fits the data for different centrality classes with minimal number of parameters. It is important here to state that the other parameterizations which was used in earlier literature has used atleast 8–10 parameters if they have to fit the data ranging from 200 GeV to 5.02 TeV simultaneously. However, using the inputs from WQM we are able to minimize the parameter numbers to 5. In fig. 3, one can see that the intermediate p_T is around 2 GeV. Above 2 GeV, the region is populated by hard particle production from high p_T QCD jets.

Figure 4 shows the data of normalized yield of charged hadrons in Au + Au collisions at 200 GeV for various centrality classes. We have fitted the experimental data [57] with our new parameterization using WQM inputs with minimal set of parameters. Here, we again find that the intermediate p_T values where both the hard and soft regions meet is around 2 GeV. Thus the value of intermediate p_T is independent of size of the colliding nucleus and is fixed for a given collision energy.

In fig. 5, we have plotted the experimental data [61] for normalized invariant yield of charged hadrons in Pb + Pb collisions at 2.76 TeV with respect to p_T. We have shown these data for seven centrality classes starting from central (0–5%) to peripheral (50–60%) collisions. Further, we have used new parameterization to fit this invariant yield. The value of parameters obtained are shown in table 1. Here an important observation is that the value of intermediate p_T is around 3.4 GeV which is higher than the intermediate p_T value at 200 GeV. Therefore, this intermediate p_T value where both hard and soft regions meet is collision energy dependent and increases with increase in collision energy.

Figure 6 shows the data of normalized yield of charged hadrons in Pb + Pb collision experiment at 5.02 TeV collision energy for various centrality classes. This is the experimental data [59] which forces the practitioner in this field to use a parametrization based on two functions. However, we assumes in our work that these two different functions are related with two different production mechanisms which exists even on RHIC energies. Only the region of soft production is small in comparison to LHC energies which can be seen by our intermediate p_T value. At 5.02 TeV, this value is around 5 GeV. Thus the region for thermal (soft) hadron production is 0 to 2 GeV at RHIC energy and it expands 0 to 5 GeV at highest LHC energy. Of course, the region of hard production increases rapidly with collision energy in comparison to soft production region.

3.2 Physical significance of parameters

In these types of parameterization, there are two things which one should keep in mind while proposing any parameterization. First, the parameters should be minimal and second thing is that the parameters used in the parameterization should have physical significance if possible. In this subsection, we have plotted all the five parameters used in our parameterization with centrality at various collisional energies for different colliding species. In fig. 7, we have plotted the parameter P_1 with centrality. Here, one can see that for a given collision energy P_1

Table 1. The fitting parameter values for charged hadrons in different colliding systems at different collision energies.

System	$\sqrt{s_{NN}}$ (GeV)	Centrality (%)	P_1	P_2	P_3 (GeV)	P_4	P_5
$p+p$	200	–	2.43341	0.00229	−0.00175	0.00539	5.41013
$p+p$	2760	–	4.96390	0.00024	0.00902	0.00064	4.50828
$p+p$	5020	–	3.85940	0.00015	0.00870	0.00039	4.40272
Cu + Cu	200	0–6	158.119	0.45448	−0.13056	1.44688	5.83805
		6–15	118.157	0.23156	−0.12774	0.70896	5.77789
		15–25	81.8937	0.11402	−0.12400	0.33179	5.64349
		25–35	54.0697	0.05008	−0.11846	0.13746	5.59300
		35–45	34.6186	0.01993	−0.11188	0.05061	5.41243
Au + Au	200	0–5	560.254	1.29140	−0.13076	4.95668	6.38872
		5–10	445.353	0.84994	−0.12936	3.16174	6.27365
		10–20	336.988	0.19685	−0.12978	0.70968	6.14995
		20–30	225.396	0.07763	−0.12679	0.26466	6.04455
		30–40	149.751	0.02005	−0.12254	0.06540	5.90898
		40–60	72.0393	0.00829	−0.10744	0.02451	5.69480
Pb + Pb	2760	0–5	1710.78	0.11925	−0.11409	0.64593	4.00928
		5–10	1388.67	0.07813	−0.11566	0.41210	4.07194
		10–20	1033.29	0.04354	−0.11574	0.21948	4.06272
		20–30	680.660	0.01946	−0.11324	0.09224	4.07689
		30–40	427.735	0.00825	−0.10756	0.03662	4.15926
		40–50	251.099	0.00296	−0.09806	0.01215	4.18388
		50–60	135.559	0.00096	−0.08565	0.00357	4.20178
Pb + Pb	5020	0–5	24557.5	0.05521	−0.00435	0.82774	3.82009
		5–10	5749.31	0.03753	−0.00466	0.39028	3.87244
		10–30	1181.44	0.01438	−0.00323	0.10552	3.96879
		30–50	478.153	0.00250	0.00064	0.01619	4.07663
		50–70	144.145	0.00028	0.00487	0.00144	4.16490

decreases with centrality and for a given centrality P_1 increases with energy. As we know that this parameter is acting like a normalization constant and related with the multiplicity of charged hadrons thus its variation with energy and centrality is trivial.

Parameter P_2 is basically related with the number of exchanged gluons among the quarks. In fig. 8, we have plotted variation of P_2 with respect to centrality at different energies. Here, we see that for a given energy the magnitude of P_2 decreases with centrality as the number of exchanged gluons decreases in peripheral collisions in comparison to central collisions. For a given centrality, P_2 weakly depends on collision energy (please keep in mind that we have plotted the graph in log scale) and slightly decreases with increasing energy. The effect of initial collision geometry, *i.e.*, the size of fireball have an effect on P_2. It can be understood in two ways: first going from central to peripheral events the size of fireball decreases and thus the P_2 decreases drastically. Second in central collisions, one can see that at 200 GeV, the size of fireball is larger in Au + Au collisions than Cu + Cu collisions and thus the value of P_2 is larger in Au + Au collisions than in Cu + Cu collisions. However in peripheral collisions, we know that the size of the fireball is the same whether it is Au + Au collisions or Cu + Cu collisions and thus the value of P_2 is same for both cases.

In fig. 9, we have plotted the parameter P_3 with respect to centrality for different collision energies. P_3 indirectly maps the collective effects of the medium. Here, one can observe that as we move from central to peripheral events the magnitude of P_3 increases and it is evident for each energy. However, as we move to 5.02 TeV, this parameter behaves abruptly and it comes close to zero values in central events and further becomes positive in peripheral events. This behaviour of P_3 at 5.02 TeV in Pb + Pb collision is similar to the P_3 values in $p+p$ collision at 2.76 and 5.02 TeV.

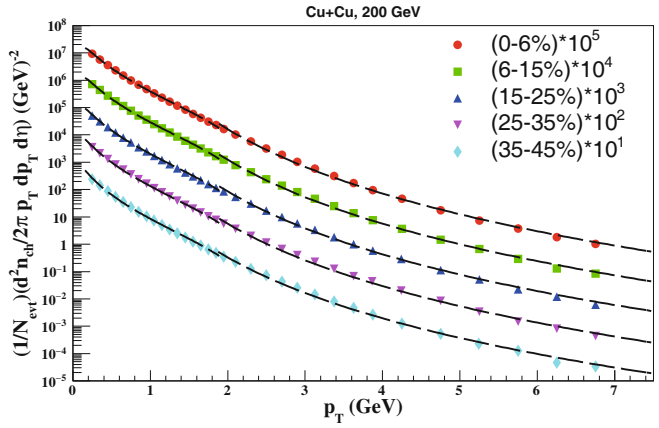

Fig. 3. (Color online) Variation of invariant yield of charged hadrons produced in Cu+Cu collisions at 200 GeV with respect to transverse momentum (p_T) in different centrality classes. The experimental data used here are taken from ref. [60].

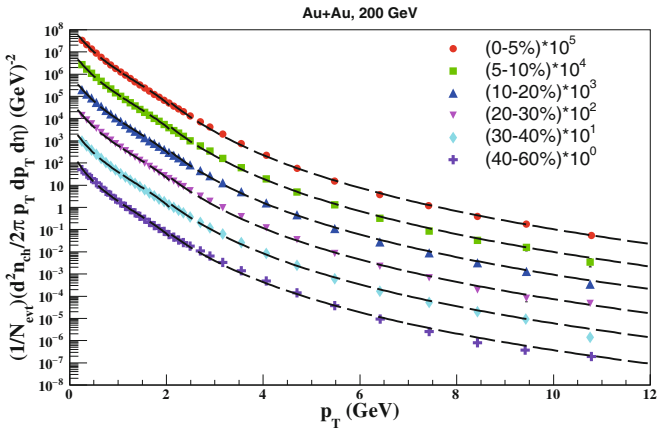

Fig. 4. (Color online) Variation of invariant yield of charged hadrons produced in Au+Au collisions at 200 GeV with respect to transverse momentum (p_T) in different centrality classes. The experimental data used here are taken from ref. [57].

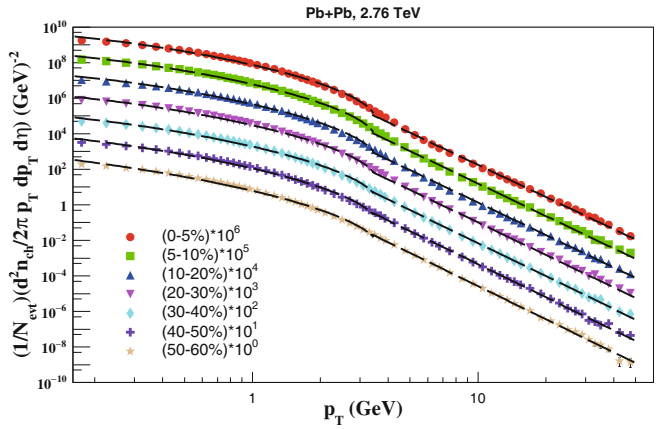

Fig. 5. (Color online) Variation of invariant yield of charged hadrons produced in Pb+Pb collisions at 2.76 TeV with respect to transverse momentum (p_T) in different centrality classes. Experimental data are taken from ref. [61].

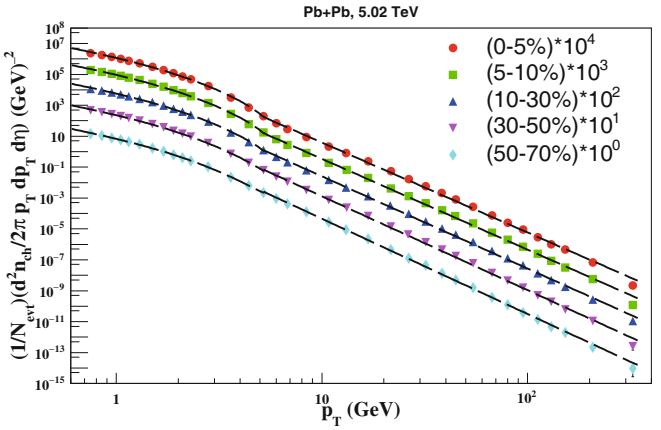

Fig. 6. (Color online)Variation of invariant yield of charged hadrons produced in Pb+Pb collisions at 5.02 TeV with respect to transverse momentum (p_T) in different centrality classes. The experimental data used here are taken from ref. [59].

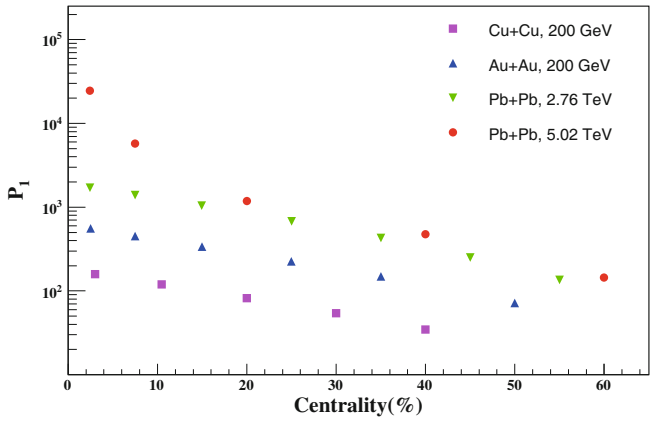

Fig. 7. (Color online) Variation of parameter P_1 with respect to centrality at three different energies 200 GeV, 2.76 TeV and 5.02 TeV. At 200 GeV we have shown the variation of P_1 for two different types of collisions, *i.e.*, Au + Au and Cu + Cu.

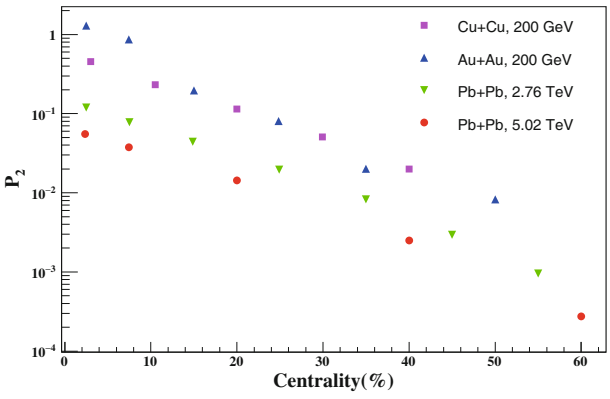

Fig. 8. (Color online) Variation of parameter P_2 with respect to centrality at three different energies 200 GeV, 2.76 TeV and 5.02 TeV. At 200 GeV we have shown the variation of P_2 for two different types of collisions, *i.e.*, Au + Au and Cu + Cu.

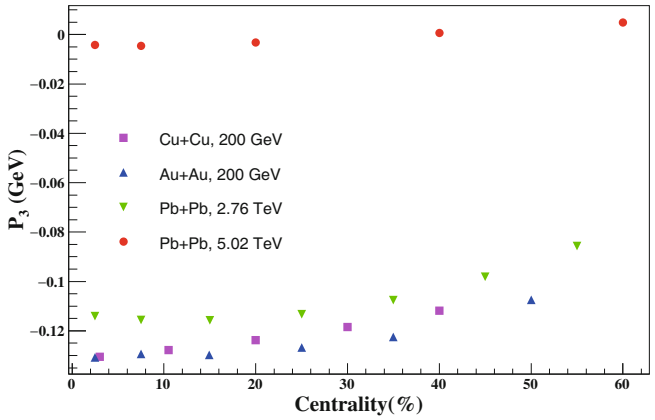

Fig. 9. (Color online) Variation of parameter P_3 with respect to centrality at three different energies 200 GeV, 2.76 TeV and 5.02 TeV. At 200 GeV we have shown the variation of P_3 for two different types of collisions, *i.e.*, Au + Au and Cu + Cu.

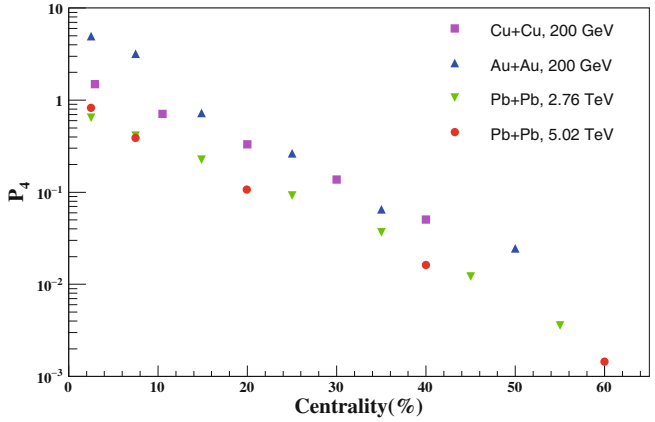

Fig. 10. (Color online) Variation of parameter P_4 with respect to centrality at three different energies 200 GeV, 2.76 TeV and 5.02 TeV. At 200 GeV we have shown the variation of P_4 for two different types of collisions, *i.e.*, Au + Au and Cu + Cu.

Figure 10 shows the variation of parameter P_4 with respect to centrality at different energies. P_4 has the same role as the parameter P_2 and thus one can understand its variation with centrality and energy accordingly. Further we have shown the variation of P_5 in fig. 11 with centrality and collision energy. Here, one can see that parameter P_5 is weakly dependent on centrality. However, it strongly depends on the collision energy. This parameter is basically related with the equilibrium of the QCD medium formed during the collisions. As its value increases from 1 to higher values, the degree of non-equilibrium increases. Thus from this figure, one can see that as we increases the collision energy, the value of P_5 decreases and tends towards 1 and thus provides a hint that the system formed during the collision is more towards equilibrium in comparison to lower energies.

In summary, we have constructed a parameterization based on the concept of two different production mechanisms in two different p_T regimes. We have started with the invariant yield distribution of charged hadrons in $p+p$ collisions using the help of modified multipomeron exchange model. We have used two different functions, *i.e.*, exponential for low p_T region and power law for high p_T region, respectively. Further, we have extended our parameterization to suitably describe the invariant yield in nucleus-nucleus collisions. For this, we have used N_q^{AB} and ν_q^{AB} from our wounded quark model and put them into the parameterization to reduce the number of free parameters from 8 (as used in the previous two functions study) to 5. We have shown the fitting of invariant yield data in $p + p$ collisions at different energies. After that we have fitted the experimental data of invariant yield in various nucleus-nucleus collisions at different energies, *i.e.*, Cu + Cu and Au + Au at 200 GeV, Pb + Pb at 2.76 and 5.02 TeV. Our parameterization based on WQM has fitted all the data simultaneously with minimal number of parameters. Finally, we have plotted the variation of different parameters with respect to centrality for different collisions and tried to find out their physical significance and their behaviour with various control parameters of collisions. In this study, we have sincerely tried to provide a parameterization which is based on quark-quark interactions with the minimal number of free parameters. We have also shown the different p_T regions, *i.e.*, low, high and intermediate and how these regions extend as we increase the collision energies.

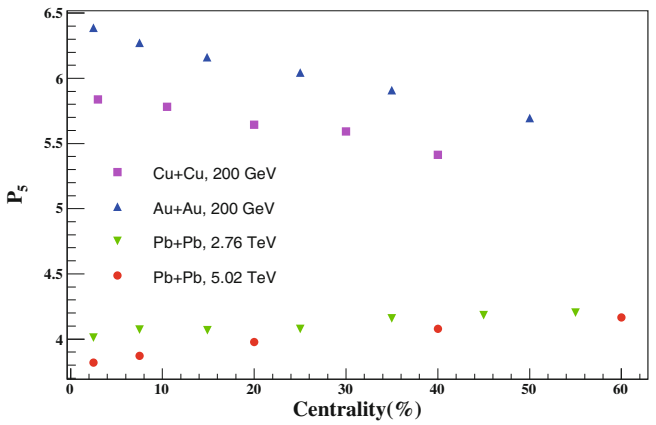

Fig. 11. (Color online) Variation of parameter P_5 with respect to centrality at three different energies 200 GeV, 2.76 TeV and 5.02 TeV. At 200 GeV, we have shown the variation of P_5 for two different types of collisions, *i.e.*, Au + Au and Cu + Cu.

PKS acknowledges IIT Ropar, India for providing an institute postdoctoral research grant. AS acknowledges the financial support obtained from UGC under research fellowship scheme in central universities. OSKC is grateful to Council of Scientific and Industrial Research (CSIR), New Delhi for providing a research grant. BKS acknowledges partial support from the FIST and PURSE of Department of Science and Technology (DST), CAS and UPE program of University Grant Commission (UGC) and from the Indian Space Research Organisation (ISRO) SSPS program, Government of India.

Data Availability Statement This manuscript has no associated data or the data will not be deposited. [Authors' comment: All the data generated during this study are contained in this article. Apart from the experimental data, which is already present online, the data generated in this study is available in table 1.]

Publisher's Note The EPJ Publishers remain neutral with regard to jurisdictional claims in published maps and institutional affiliations.

References

1. C.P. Singh, Phys. Rep. **236**, 147 (1993).
2. P. Braun-Munzinger, K. Redlich, J. Stachel, arXiv:nucl-th/0304013.
3. I.M. Dremin, J.W. Gary, Phys. Rep. **349**, 301 (2001).
4. J. Sollfrank, P. Huovinen, M. Kataja, P.V. Ruuskanen, M. Prakash, R. Venugopalan, Phys. Rev. C **55**, 392 (1997).
5. N. Xu, Z. Xu, Nucl. Phys. A **715**, 587 (2003).
6. P. Braun-Munzinger, J. Stachel, J.P. Wessels, N. Xu, Phys. Lett. B **344**, 43 (1995).
7. P. Braun-Munzinger, J. Stachel, J.P. Wessels, N. Xu, Phys. Lett. B **365**, 1 (1996).
8. T. Sjöstrand, M. van Zijl, Phys. Rev. D **36**, 2019 (1987).
9. K. Kinoshita, H. Noda, T. Tashiro, M. Mizouchi, Z. Phys. C Part. Fields **4**, 103 (1980).
10. STAR Collaboration (B.I. Abelev *et al.*), Phys. Rev. C **79**, 034909 (2009).
11. PHENIX Collaboration (A. Adare *et al.*), Phys. Rev. C **83**, 024909 (2011).
12. T.S. Biro, B. Muller, Phys. Lett. B **578**, 78 (2004).
13. G. Wilk, Z. Wlodarczyk, Eur. Phys. J. A **40**, 299 (2009).
14. T. Osada, G. Wilk, Phys. Rev. C **77**, 044903 (2008).
15. W.M. Alberico, A. Lavagno, P. Quarati, Eur. Phys. J. C **12**, 499 (2000).
16. B. De, S. Bhattacharyya, G. Sau, S.K. Biswas, Int. J. Mod. Phys. E **16**, 1687 (2007).
17. PHENIX Collaboration (A. Adare *et al.*), Phys. Rev. C **83**, 064903 (2011).
18. CMS Collaboration (S. Chatrchyan *et al.*), Eur. Phys. J. C **72**, 2164 (2012).
19. C. Tsallis, J. Stat. Phys. **52**, 479 (1988).
20. C. Tsallis, R.S. Mendes, A.R. Plastino, Physica A **261**, 534 (1998).
21. H. Zheng, L. Zhu, Adv. High Energy Phys. **2015**, 180491 (2015).
22. Kapil Saraswat, Prashant Shukla, Venktesh Singh, J. Phys. Commun. **2**, 035003 (2018).
23. UA 2 Collaboration (R. Ansari *et al.*), Z. Phys. C **36**, 175 (1987).
24. UA 2 Collaboration (J.A. Appel *et al.*), Phys. Lett. B **165**, 441 (1985).
25. T. Åkesson, H. Bengtsson, Phys. Lett. B **120**, 233 (1983).
26. A. Kumar, P.K. Srivastava, B.K. Singh, C.P. Singh, Adv. High Energy Phys. **2013**, 352180 (2013).
27. A. Kumar, B.K. Singh, P.K. Srivastava, C.P. Singh, Eur. Phys. J. Plus **128**, 45 (2013).
28. O.S.K. Chaturvedi, P.K. Srivastava, A. Kumar, B.K. Singh, Eur. Phys. J. Plus **131**, 438 (2016).
29. C.P. Singh, M. Shyam, S.K. Tuli, Phys. Rev. C **40**, 1716 (1989).
30. M. Shyam, C.P. Singh, S.K. Tuli, Phys. Lett. B **164**, 189 (1985).
31. C.P. Singh, M. Shyam, Phys. Lett. B **171**, 125 (1986).
32. O.S.K. Chaturvedi, P.K. Srivastava, A. Singh, B.K. Singh, Eur. Phys. J. Plus **132**, 430 (2017).
33. O.S.K. Chaturvedi, P.K. Srivastava, Arpit Singh, B.K. Singh, Eur. Phys. J. A **54**, 46 (2018).
34. S. Eremin, S. Voloshin, Phys. Rev. C **67**, 064905 (2003).
35. PHENIX Collaboration (A. Adare *et al.*), Phys. Rev. C **93**, 024901 (2016).
36. PHENIX Collaboration (S.S. Adler *et al.*), Phys. Rev. C **89**, 044905 (2014).
37. STAR Collaboration (J. Adams *et al.*), Phys. Rev. C **72**, 014904 (2005).
38. STAR Collaboration (B.I. Abelev *et al.*), Phys. Rev. C **81**, 044902 (2010).
39. STAR Collaboration (J. Adams *et al.*), Phys. Rev. Lett. **92**, 052302 (2004).
40. STAR Collaboration (J. Adams *et al.*), Phys. Rev. Lett. **95**, 022301 (2005).
41. P. Bożek, W. Broniowski, Phys. Rev. C **96**, 014904 (2017).
42. A. Bialas, W. Czyz, L. Lesniak, Phys. Rev. D **25**, 9 (1992).
43. V.V. Anisovich, V.M. Shekhter, Nucl. Phys. B **55**, 455 (1973).
44. V.V. Anisovich, M.N. Kobrinskii, J. Nyiri, Yu.M. Shabelskii, Sov. Phys. Usp. **27**, 12 (1984).
45. J. Nyiri, Int. J. Mod. Phys. A **18**, 2403 (2003).
46. H.J. Lipkin, Phys. Lett. B **116**, 175 (1982).
47. S. Fernbach, R. Serber, T.B. Taylor, Phys. Rev. **75**, 1352 (1949).
48. T.F. Hoang, B. Cork, H.J. Crawford, Z. Phys. C **29**, 611 (1985).
49. N. Armesto, D.A. Derkach, G.A. Feofilov, Phys. At. Nucl. **71**, 2087 (2008).
50. A. Capella, U.P. Sukhatme, C.-I. Tan, J. Tran Thanh Van, Phys. Lett. B **81**, 68 (1979).
51. A.B. Kaidalov, Phys. Lett. B **116**, 459 (1982).
52. V.A. Abramovskii, V.N. Gribov, O.V. Kancheli, Sov. J. Nucl. Phys. **18**, 308 (1974).
53. A.B. Kaidalov, K.A. Ter-Martirosyan, Phys. Lett. B **117**, 247 (1982).
54. A.B. Kaidolov, Sov. J. Nucl. Phys. **45**, 902 (1987).
55. Yu.M. Shabelski, Z. Phys. C **57**, 409 (1993).
56. J. Schwinger, Phys. Rev. **82**, 664 (1951).
57. STAR Collaboration (J. Adams *et al.*), Phys. Rev. Lett. **91**, 172302 (2003).
58. CMS Collaboration (S. Chatrchyan *et al.*), Eur. Phys. J. C **72**, 1945 (2012).
59. CMS Collaboration (V. Khachatryan *et al.*), J. High Energy Phys. **2017**, 39 (2017).
60. PHOBOS Collaboration (B. Alver *et al.*), Phys. Rev. Lett. **96**, 212301 (2006).
61. ALICE Collaboration (B. Abelev *et al.*), Phys. Lett. B **720**, 52 (2013).